Huang, Zhi-Cheng; Hwung, Hwung-Hweng; Hsiao, Shih-Chun

Measurement of the Near-Bed Turbulence in a Laboratory Surf Zone

MEASUREMENT OF THE NEAR-BED TURBULENCE IN A LABORATORY SURF ZONE

Zhi-Cheng Huang[1], Hwung-Hweng Hwung[2] and Shih-Chun Hsiao[3]

[1] Ph. D. Candidate, Department of Hydraulic and Ocean Eng., National Cheng Kung University
1 Ta-Hsueh Road, Tainan 701, Taiwan (R.O.C.), e-mail: n8893107@ccmail.ncku.edu.tw
[2] Professor, Department of Hydraulic and Ocean Eng., National Cheng Kung University
1 Ta-Hsueh Road, Tainan 701, Taiwan (R.O.C.), e-mail: hhhwung@mail.ncku.edu.tw
[3] Assistant Professor, Department of Hydraulic and Ocean Eng., National Cheng Kung University
1 Ta-Hsueh Road, Tainan 701, Taiwan (R.O.C.), e-mail: *schsiao@mail.ncku.edu.tw*

ABSTRACT

Surf-zone turbulence, primarily generated by wave roller and water splash up process, dominates sediment transport and energy dissipation. The turbulence in crest region may further penetrate into wave boundary layer and change the inside flow characteristics. This study presents a measurement of the near-bed turbulence in the surf zone using a modified high-spatial-resolution Particle Image Velocimetry (PIV) system. The velocities were measured at two positions, spilling point (p1) and water splashing point (p2), in the surf zone due to a presumption of different turbulence penetration levels in these two locations. The ensemble-averaged method was employed to decompose the turbulence and mean flow motion by repeating the same experiments for more than thirty runs. It is found that the turbulence intensity is larger in p2 than that in p1. This reflects that the spilling process is a local phenomenon in the outer surf zone where lesser penetration of turbulence occurs. In p2, a relative large turbulent vortical structure and numerous small velocity fluctuations were observed. The turbulences were produced from the previous passing wave due to the smooth boundary condition. This finding further suggests a rapid burst of shear stress and turbulent intensity, which significantly contribute to a suspension of sediment.

Keywords: boundary layer, wave breaking, surf zone, turbulence, PIV

1. INTRODUCTION

Gravity waves shoal into shallow water with the increase of nonlinearity, leading the steepening of wave crest and flattening wave trough. The wave profile becomes unstable and wave breaking occurs. The hydrodynamics of breaking waves significantly relate to sediment transport especially for that in the near-bed region. It is known that surf-zone turbulence is primarily produced in the wave crest region and secondarily in the bottom layer (Christensen et al., 2002). Although strong turbulence is generated by wave roller in the crest region, they may further penetrate into the wave boundary layer, thus changing the inside flow characteristics and leading high sediment suspension.

Because the WBL is very thin, fewer measurements of flow motion in the WBL have been done. In the past, some field and laboratory measurements of WBL for breaking wave were conducted using hot film anemometer and Laser Doppler Velocimetry. In addition, some investigations were made in a oscillating water tunnel (Jonsson and Carlsen, 1976; Hino et al., 1983) and the stretched turbulence was simulated by artificial grids placed a certain distance above the bottom due to that the wave breaking can not be modelled directly (Fredsøe et al., 2003).

Measurements of boundary layer flow in a laboratory wave flume are difficult to

perform and rarely have been made. Deigaard et al. (1991) used a hot film probe to measure the temporal variation of bottom shear stress under breaking waves on a smooth sloping bottom. Cox et al. (1996) employed the LDV technique to measure the velocities under spilling breakers on a rough, impermeable 1:35 slope, and the bottom shear stress and bottom roughness were estimated as well. Recently, Lin and Hwung (2002) used the LDV technique to measure the WBBL of shoaling waves in the pre-breaking zone. They found that the boundary layer flow was similar to a laminar flow and that the Stokes layer thickness remained constant in the pre-breaking zone.

Prior to this study, the turbulent motion near the wall region in the surf zone has not been examined using efficient and non-intrusive measuring instruments, such as a particle image velocimeter (PIV). According to a wide literature survey, this study is the first to investigate the surf-zone WBBL using PIV in an ordinary wave flume. Because the viscous boundary layer thickness was approximately 1 mm, a macro photography technique was applied in the ordinary PIV system to improve the optical magnification. This allows 10 points of velocities to be measured simultaneously near the wall region. The measurement also relies on other techniques, such as delivery of the light sheet beneath the bed, a high concentration of seeding particles and minimum depth of field of camera. The velocity profiles and turbulence level in the outer and inner surf zone also were examined. The results of a traditional cross-correlation based PIV analysis show that the spatial distributions of velocities in the surf-zone boundary layer can be measured efficiently and robustly by the presented techniques. This method also provides novel evidence for the existence of the turbulent structure in the smooth wall region.

2. EXPERIMENTS

Figure 1 shows the experimental facilities and setup. The experiments were conducted in a glass side-walled wave flume (25 m long x 30 cm wide x 70 cm deep) at the Tainan Hydraulics Laboratory. Progressive regular waves were generated by a piston-type wavemaker located at one end of the flume. A 1/20 transparent sloping bottom made of polymethyl methacrylate with a transmission rate up to 95% and an average surface roughness 0.52 μm was placed at the tail of the flume. The velocities near the bottom boundary in the surf zone were measured by the PIV in two fields of view (FOV) at two positions (p1 and p2) in the surf zone. The maximum frame capturing rate of the CCD camera (TSI, USA, Powerview 2M, 1600×1192 pixels, 16-bits) was 30 frames per second (fps). The macro photography technique was applied in the PIV system. Because the boundary layer thickness on a smooth bottom is O (1) mm, a micro-lens (60 mm, f /2.8 D, Nikon Micro-Nikkor, Japan) and a magnifying glass were used to improve the insufficient resolution of original camera of the PIV system. The optical magnification was up to 1.09. The modified spatial resolution of the CCD camera was 6.7953 μm / pixel. The camera was installed on a movable three-dimensional optical flat table controlled by digital-server motors. The optical table could move with a precision of 0.02 mm, which allowed the CCD to focus accurately.

A dual Nd:YAG laser system (New Wave, USA, 120 mJ/pulse, 30 Hz, 532 nm wavelength) was used to illuminate the measuring section. A mirror was mounted at a 45° angle under the transparent sloping bottom. The light sheet was formed from the laser beam passing through a cylindrical lens (f15.0 mm) and a spherical lens (f0.5 m) and then being reflected by the mirror to the measuring section. After testing, the depth-of-field of the camera was adjusted to minimum with a magnitude of 1 mm. The water in the wave flume was seeded with nearly neutrally buoyant uncoated and silver coated hollow glass spheres particle (TSI, normal mean diameter is ~10 μm, density is ~1.05 g/cm^3) to enhance the illumination

efficiency during the PIV measurements. A sufficient concentration of tracer particles was placed near the bottom region before each test run.

The wave profiles were measured by three capacitance-type wave gages with a sampling rate of 50 Hz. The data was recorded by a data acquisition board controlled by Labview (National Instruments). The first wave gauge was set in the constant depth water 6 m away from the wave paddle to examine the incident wave condition. The second gauge was at $x = -39$ cm in the pre-breaking zone and the third was set at $x = 0$ cm (p1) and $x = 25$ cm (p2). The local still water depth, d, was 5.3 cm at p1 and 4.05 cm at p2. Monochromatic waves with an incident wave period of 1.0 second and an incident wave height of 3.0 cm were generated in the constant depth water of 0.36 m. The corresponding offshore surf similarity parameter (Battjes, 1974) is 0.036, and the breaking wave was obviously a spilling type. The local average wave height was 3.69 cm at p1 and 2.75 cm at p2. Position 1 was at the bore established region in the outer surf zone and p2 was at the inner surf zone according to the description given by Lin and Hwung (1992).

The velocity field was calculated based on the zero-padded fast-Fourier-transform (FFT) cross-correlation and the three points Gaussian peak in the TSI's Insight. Each pair of images was processed from an interrogation window size of 32×32 pixels using 50% overlap. Only 1600 × 1184 pixels of the images were used to calculate. The final data set contains a 99 × 73 grid of velocity vectors on a 16-pixel square grid with a spatial resolution of 0.1087×0.1087 mm^2. A global range filter and a standard deviation filter were used to remove spurious vectors. Then, the missing velocities were interpolated using the Kriging method (Agterberg, 1970; Chang and Liu, 1999).

Because each breaking wave within the wave train is slightly different in the surf zone, it is better to decompose the mean and fluctuating velocities using the ensemble-average method by repeating the same experiments instead of the moving-average or phase-average methods. To measure the flow velocity under the same wave phase among different test runs, the second wave gauge was used as a reference external trigger signal. A threshold of trigger was set to begin the measuring procedure of the surface elevation. Then, the exposure time of the images and the illumination time of the laser were carefully controlled by TTL signals generated from a time counter connected synchronously to the data acquisition board. After considering the experimental conditions, the time interval between two successive laser pulses was set at 0.25 ms. The camera frame and laser illumination rates were set at 20 Hz, yielding a PIV velocity field rate of 10 Hz and hence a temporal resolution of 10 phases per second. The same experiments were repeated 30 times, and the velocity fields were measured for 12 s in each test run. To increase the measured phases, another series of test runs was conducted by setting a time delay of 0.05 s of PIV relative to the first series of experiments. Figure 2 shows the combined results of the ensemble-averaged horizontal velocity at p2 at a vertical position of $z_m = 1.4678$ mm ($z_m = z + d$ is defined as positive upward with $z_m = 0$ on the fixed bottom and d = the still water depth) for the two series (without and with time delay). Clearly, this time-delay method produced twice the resolution (20 wave phases per second) in the ensemble-averaged results.

The ensemble-averaged mean streamwise (horizontal) velocity, U, and vertical velocity, W, are defined as:

$$U = \langle u \rangle_N = \frac{1}{N} \sum_{j=1}^{N} u_j \ ; \ W = \langle w \rangle_N = \frac{1}{N} \sum_{j=1}^{N} w_j \ , \qquad (1)$$

where u and w are the measured instantaneous streamwise and vertical velocities, respectively; the symbol $\langle \ \rangle$ represents the ensemble average; j denotes the j^{th} experiment; and N is the total number of experiments. The measured turbulent component of the flow is then defined as:

$$u' = u - U \ ; \ w' = w - W \ , \qquad (2)$$

where u' and w' denote the horizontal and vertical velocity fluctuations, respectively. Because only two velocity components were measured, the turbulent kinetic energy (TKE) is defined as:

$$k = \frac{1.33}{2}\langle u'u' + w'w' \rangle_N , \qquad (3)$$

where the coefficient 1.33 was obtained from the assumption that breaking waves have characteristics similar to those of the plane wake (Svendsen, 1987). Presumably, the mean velocity field is convergent as $N \to \infty$. In practice, the mean flow reaches a convergent state after the experiment is repeated a sufficient number of times. Convergence tests of the measured velocities and TKE were conducted at crest and trough phases in the two measuring positions. Relative errors of U and k at a specific point are given by:

$$dV_N = (U_N - U_{30})/U_{30}; \quad N = 1,2,\cdots,30 \qquad (4)$$

$$dk_N = (k_N - k_{30})/k_{30}; \quad N = 1,2,\cdots,30 . \qquad (5)$$

Two points, located inside (z_m = 0.99 mm) and outside (z_m = 4.57 mm) the boundary layer under the trough phase at p2, were used for the statistical convergence test of the ensemble-averaged results. The relative errors of the averaged streamwise velocity and turbulent kinetic energy density are presented in Figure 3, respectively. The variations of dV_N and dk_N were < 0.05 for $N \geq 10$ and $N \geq 19$. All averaging results in this study were computed using N > 25, confirming that it is sufficient to determine the ensemble-averaged quantities.

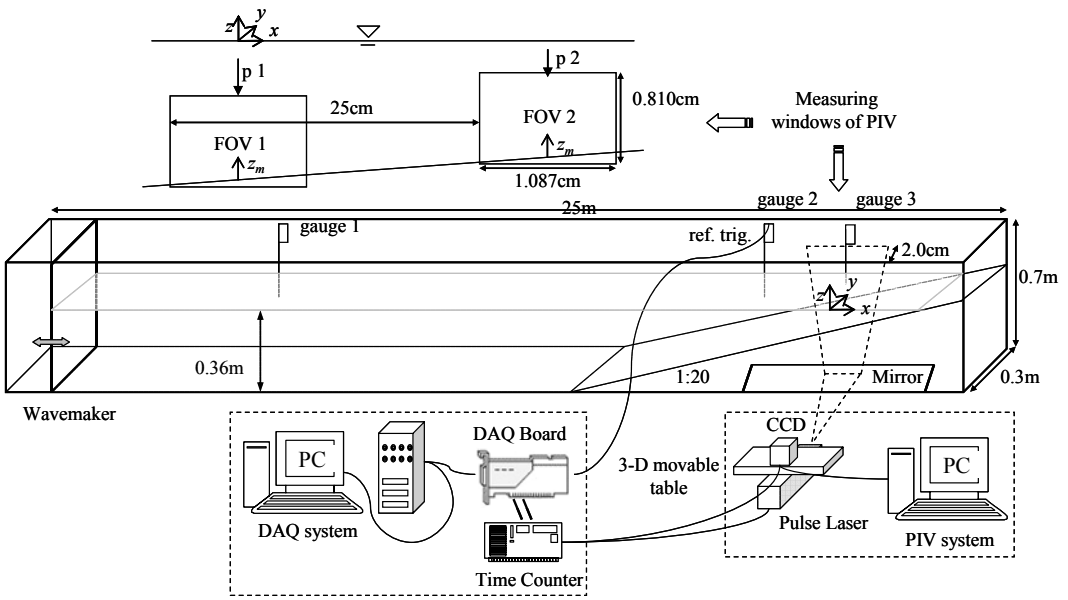

Figure 1. Experimental facilities and setup

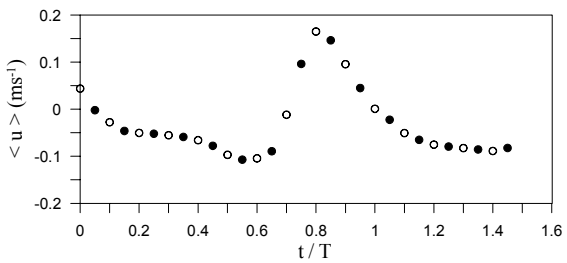

Figure 2. Combined ensemble-averaged horizontal velocities for two series of test runs at p2, z_m = 1.4678 mm. Hollow circles: without time delay (original series); filled circles: with time delay of 0.05 sec referenced to the original series.

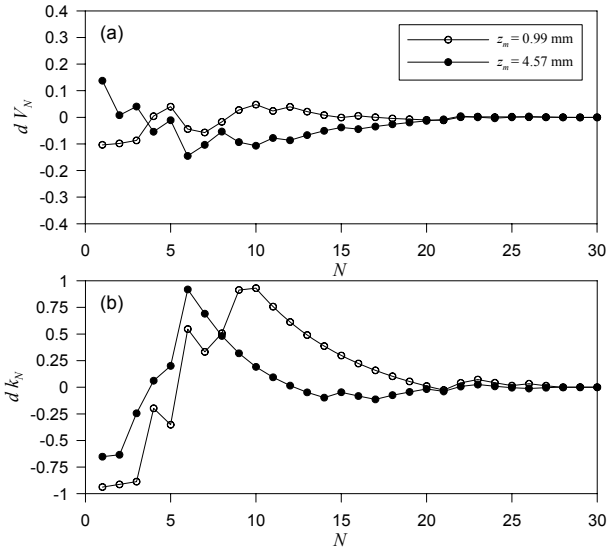

Figure 3. Statistical convergence tests at p2. (a) dV_N ; (b) dk_N . The data phase is at t/T = 1.6.

3. RESULTS AND DISCUSSIONS

3.1 The ensemble-averaged flow

Figure 4 and Figure 5 show the measured temporal variations of the surface elevations, η ($\bar{\eta}$ is the mean water level), and the vertical profiles of the ensemble-averaged streamwise velocity at p1 and p2, respectively. The vertical measuring position, z_m ($z_m = z + d$), was normalized by the Stokes layer thickness, $\delta = \sqrt{\nu T / \pi}$ (ν is the kinematic viscosity of water and T is the oscillating period). These profiles have characteristics similar to those of typical velocity profiles of boundary layer flow in the nearly breaking zone given by Lin and Hwung (2002). Overshooting behavior occurred in the near-bottom region under the crest phase (t/T = 0.5 at p1 and t/T = 0.8 at p2). The velocity deficit and velocity gradient also occurred close to the bed due to the existence of the viscous wall boundary condition. The velocities under the crest phase were larger than those under the trough phase at p1, likely because of the increase of nonlinearity (i.e., sharpened wave crest and flattened wave trough) due to the wave shoaling effect (Lin and Hwung, 2002). However, the distributions of the onshore and offshore components differed from those in the pre-breaking zone. The dominant direction of the flow motion was onshore in the pre-breaking region but changed to offshore in the surf zone. Strongly asymmetric distribution of onshore and offshore components also occurred at p2. In Addition, the crest velocities at the boundary layer at p2 were smaller than those under the trough phase.

3.2 Turbulent kinetic energy density

Figure 6 presents the temporal variations of the vertical profile of the TKE density. The order of magnitude of the TKE at p1 was relatively small because of the smooth bottom condition (~10^{-5} m^2s^{-2}). The TKE at p2 was larger than the TKE at p1, and the maximum TKE occurred under the wave trough phases (t/T = 1.3 at p1 and t/T = 1.6 at p2). The bottom was so smooth that the external turbulence was considered the dominant source for distributing the TKE. This finding reflects previous observations that the spilling process is a

local phenomenon in the outer surf zone and that the penetration of turbulence is lesser in the outer surf zone (p1) than in the inner surf zone (p2) (Lin and Hwung, 1992; Lin and Liu, 1998). These results further suggest that the residual turbulence diffused from the crest region of the passed wave was able to penetrate to the WBBL in the inner surf zone and change the inside characteristics of flow motion, such as the increase of turbulent intensity and bottom shear stress.

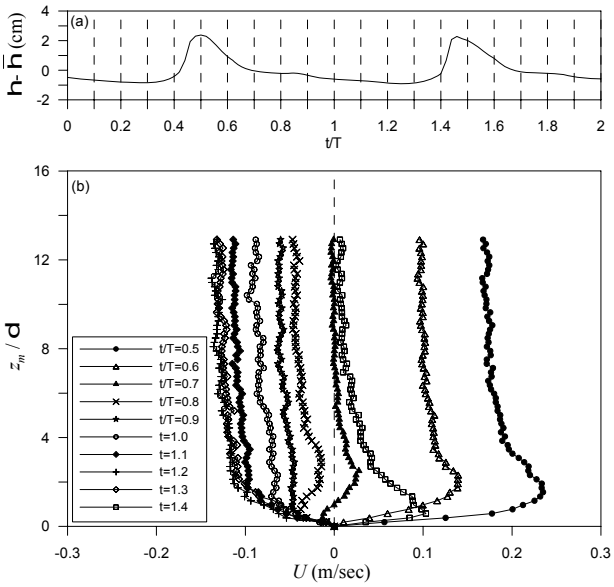

Figure 4. Temporal variations of (a) the surface profile and (b) the vertical distributions of the ensemble-averaged streamwise velocity at p1.

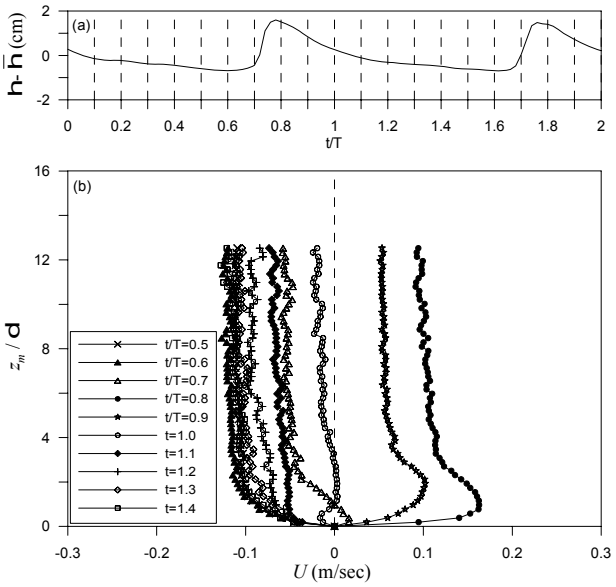

Figure 5. Temporal variations of (a) the surface profile and (b) the vertical distributions of the ensemble-averaged streamwise velocity at p2.

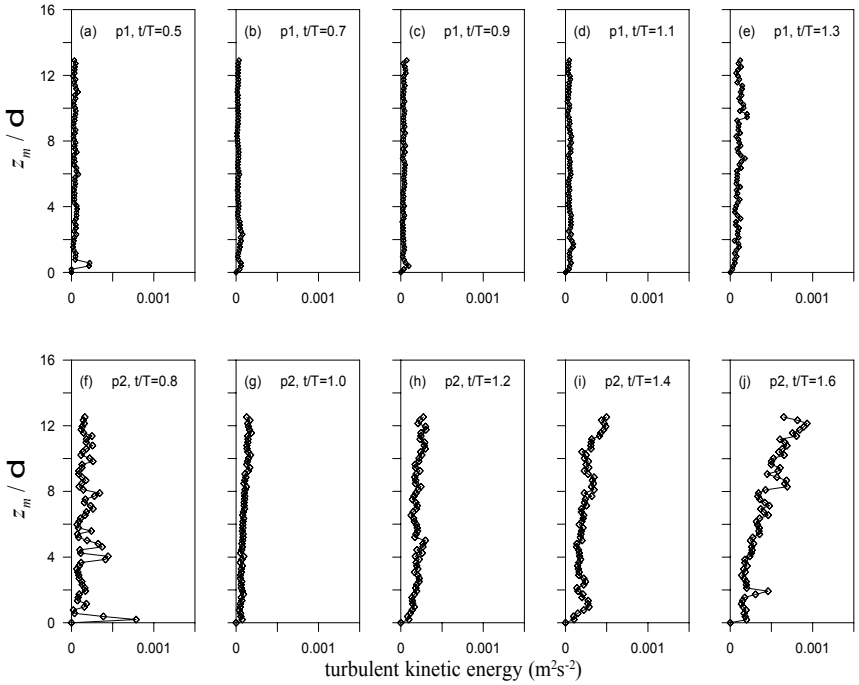

Figure 6. Temporal variations of the vertical distributions of the turbulent kinetic energy density at p1 (a~e) and at p2 (f~j).

3.3 Spatial distribution of velocity and vorticity fields

An advantage of the PIV measurement is its ability to reveal the spatial distribution of the turbulent structures. The data set contained remarkable evidence of the change of the WBBL caused by the penetrated turbulent vortical structures. The vortical structure could not be measured with each passing wave. Thus, the spatial turbulent structure could not be observed in the ensemble-averaged quantities (Cox and Kobayashi, 2000). Figure 7 shows a sample of the instantaneous velocity field superimposed on its corresponding vorticity distribution, which is defined as $\omega = 0.5(\partial w/\partial x - \partial u/\partial z)$. The flow was turbulent and there was a relatively large vortical structure (~5 cm diameter, positive value, counterclockwise, located at 245 mm < x < 249 mm) and numerous small velocity fluctuations. The turbulence was produced from the previous passing wave due to the smooth boundary condition. Figure 8 shows the corresponding distribution of the turbulent fluctuations and the turbulent vorticity ($\omega' = 0.5(\partial w'/\partial x - \partial u'/\partial z)$). The mean flow direction of the wave component was offshore with a magnitude of 2 cms^{-1}. This turbulent event consisted of a relatively large eddy with positive turbulent vorticity surrounded by many small eddies with negative vorticity. This finding further suggests a rapid burst of shear stress and turbulent intensity, which may significantly contribute to the suspension of sediment.

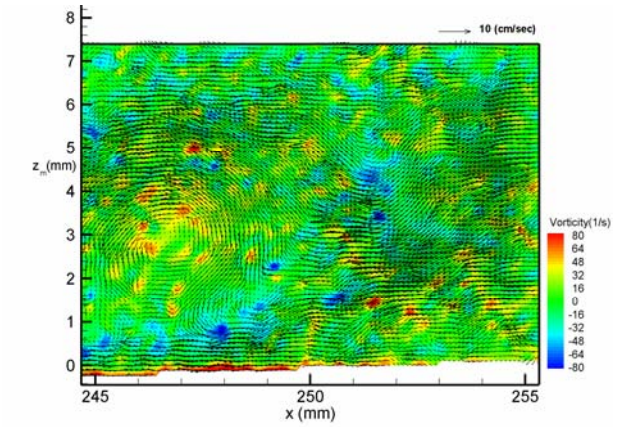

Figure 7. Example of the instantaneous velocity field superimposed on the vorticity distribution at p2 at t/T = 3.05.

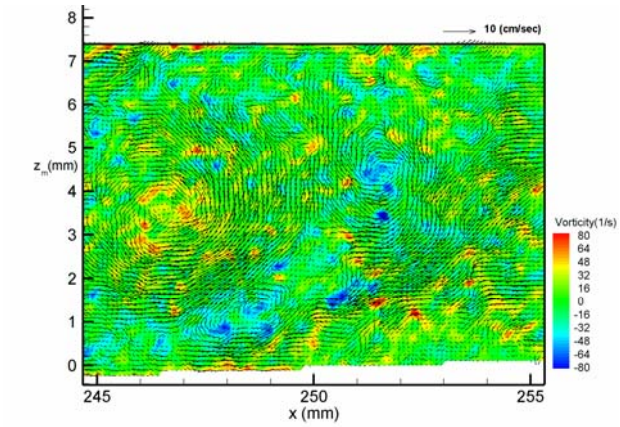

Figure 8. The distribution of the velocity fluctuations (u' and w') and the turbulent vorticity field corresponding to Figure 2.

4. CONCLUSIONS

Measurement of the surf-zone turbulence in the wave boundary layer was performed by PIV. Since the spatial resolution of an original PIV is not large enough, the optical magnificence of the CCD was improved more than one to achieve a resolution of 6.7953 μm / pixel, which allows a simultaneous measurement of the velocity profiles of boundary layer flow. We used the ensemble-averaged method for turbulence decomposition by repeating the same experiments for more than thirty runs.

It is found that the turbulence intensity is larger at the spilling point of braking wave (p1). This reflects that the spilling process is a local phenomenon in the outer surf zone where lesser penetration of turbulence occurs. The bottom is a smooth condition that the external turbulence is considered the dominative source for distributing the TKE. These results further suggest that the residual turbulence diffused from the crest region of the passed wave is able to penetrate to the WBBL in the inner surf zone and change the inside characteristics of flow

motion, such as the increase of turbulent intensity and bottom shear stress.

The data set contained remarkable evidence of the change of the WBBL caused by the penetrated turbulent vortical structures in the splashing point (p2). A relative large turbulent vortical structure and numerous small velocity fluctuations were observed. The turbulences were produced from the previous passing wave due to the smooth boundary condition. This finding further suggests a rapid burst of shear stress and turbulent intensity, which significantly contribute to a suspension of sediment.

ACKNOWLEDGMENTS

The authors would like to express sincere gratitude to the National Science Council in Taiwan for the financial support (Grant No: NSC 94-2611-E-006-014, NSC 96-2628-E-006 - 249 –MY3). They appreciate the Tainan Hydraulics Laboratory to provide the facilities and instrumentations. They also thank Dr. K.S. Hwang and Mr. W.Y. Hsu for their assistances in consultation and conducting the experiments.

REFERENCES

Agterberg FP (1970) Autocorrelation functions in geology. Geostatistics, edited by Merriam DF.

Battjes JA (1974) Surf similarity. In Proceedings of 14th International Conference on Coastal Engineering,

Copenhangen, ASCE, 447–465

Chang KA, Liu PLF (1999) Experimental investigation of turbulence generated by breaking waves in water of intermediate depth. Phys Fluids 11(11):3390–3400

Agterberg, F.P., 1970. Autocorrelation functions in geology. Geostatistics.

Battjes, J.A., 1974. Surf similarity, 14th International Conference on Coastal Engineering. ASCE, Copenhangen, pp. 447-467.

Chang, K.A. and Liu, P.L.F., 1999. Experimental investigation of turbulence generated by breaking waves in water of intermediate depth. Phys Fluids, 11(11): 3390-3400.

Christensen, E.D., Walstra, D.J. and Emerat, N., 2002. Vertical variation of the flow across the surf zone. Coastal Eng, 45(1): 165-198.

Cox, D.T. and Kobayashi, N., 2000. Identification of intense, intermittent coherent motions under shoaling and breaking waves. J Geophys Res, 105(C6): 14223-14236

Cox, D.T., Kobayashi, N. and Okayasu, A., 1996. Bottom shear stress in the surf zone. J Geophys Res, 101(C6): 14337-14348.

Deigarrd, R., Mikkelsen, M.B. and Fredsøe, J., 1991. Measurements of the bed shear stress in a surf zone. 73, ISVA Tech Univ Denmark.

Fredsøe, J., Sumer, B.M., Kozakiewicz, A., Chua, L.H.C. and Deigaard, R., 2003. Effect of externally generated turbulence on wave boundary layer. Coastal Eng, 49: 155-183.

Hino, M., Kashiwayanagi, M. and Hara, T., 1983. Experiments on the turbulent statistics and structure of reciprocating oscillatory flows. J Fluid Mech, 131: 363-400.

Jonsson, I.G. and Carlsen, N.A., 1976. Experimental and theoretical investigations in an oscillatory turbulence boundary layer. J Hydra Res, 14: 46-60.

Lin, C. and Hwung, H.H., 1992. External and internal flow fields of plunging breaker. Exp Fluids, 12: 229-237.

Lin, C. and Hwung, H.H., 2002. Observation and measurement of the bottom boundary layer flow in the prebreaking zone of shoaling waves. Ocean Eng, 29: 1479-1502.

Lin, P. and Liu, P.L.F., 1998. A numerical study of breaking waves in the surf zone. J Fluid Mech, 359: 239-264.
Svendsen, I.A., 1987. Analysis of surf zone turbulence. J Geophys Res, 92(C5): 5115-5124.